Doppler Signature Analysis in Over-The-Horizon Radar for Target with Time-Varying Velocity

Yimin D. Zhang
Department of Electrical and Computer Engineering
Temple University
Philadelphia, PA 19122, USA

Braham Himed
Distributed RF Sensing Branch
Air Force Research Laboratory
WPAFB, OH 45433, USA

***Abstract*—Doppler signature analysis of targets, particularly micro-multipath signals, plays an important role in target trajectory analysis and tracking in over-the-horizon radar. In this paper, we examine the Doppler signatures of micro-multipath signals for a target that moves with a constant altitude but its velocity varies due to, for example, turbulence. We first describe the effect of such velocity variation in the resulting Doppler signatures under the micro-multipath model. Noticing that the velocity variation changes the Doppler signatures of all micro-multipath components in a similar manner, the self-stationarization approach is applied to provide a robust Doppler difference estimation.**

Keywords: Doppler analysis, radar signal processing, over-the-horizon radar, target localization, time-frequency analysis.

I. Introduction

Sky-wave over-the-horizon radar (OTHR) is an early warning system that provides long-range wide-area surveillance capability beyond the limit of the earth horizon by exploiting ionospheric reflections [1–5]. One of the important tasks in OTHR operation is the estimation of target parameters [6–10]. Among these parameters is the target altitude, which is useful for target recognition and classification, and has been the subject of extensive studies [6, 7, 11–14]. Altitude estimation using a matched-field approach [6, 11] exploits multiple OTHR dwells and the altitude-dependent structure of the micro-multipath (also known as local-multipath) rays resulting from reflections that are local to the target. A generalized altitude estimation approach considered the effect of random ionospheric and target motion which degrades the dwell-to-dwell predictability of target returns [7]. Target altitude estimation exploiting multipath propagation model was experimentally validated in [12].

A different approach was taken through the time-frequency analysis of the micro-Doppler signatures which are, in general, non-stationary. Such analyses have allowed for the estimation and tracking of target vertical velocity and target altitude [8, 13, 15–18]. For maneuvering targets, the Doppler difference of the received micro-multipath signals is associated with the target elevation velocity. As such, resolved time-frequency analysis of the micro-Doppler signatures enables estimation and tracking of target elevation velocity and altitude.

Recently, it is revealed that, when a target maintains a constant altitude and moves with a constant velocity, the micro-Doppler frequencies can be considered as parallel linear frequency modulated (LFM, also known as chirp) signatures [19–22]. Such signals can be effectively analyzed using, e.g., the fractional Fourier transform [23, 24].

In practice, flying targets may experience velocity perturbations due to flight dynamics and the external atmospheric environment [25–27]. As a result, the micro-multipath Doppler signatures of a target may deviate from the parallel LFM Doppler signal model originally developed for targets without considering such perturbations. In this paper, we analyze the effect of target velocity perturbation on the resulting Doppler signatures. We provide general mathematical formulations followed by two specific cases, namely, piecewise constant target velocity and sinusoidal velocity changes. Depending on the severity of a velocity perturbation, the micro-Doppler signatures may no longer be considered as LFM signals. In this case, utilizing the parallel property of the micro-Doppler signatures, the self-stationarization technique [28] is exploited to convert the micro-Doppler components into sinusoids which can be conveniently analyzed using Fourier transform or sparsity-based spectrum analysis methods. Simulation results verify the effectiveness of the proposed technique.

II. Signal Model

A. Multipath Propagation Geometry

OTHR systems are typically operated in a pseudo-monostatic mode in which the separation between the transmit array and the receive array is much smaller than the surveillance range. In this paper, we consider an air target of interest that maintains a constant altitude whereas its horizontal velocity is perturbed by, for example, wind turbulence.

The problem is considered in a simplified flat-earth model [8] and the propagation paths are illustrated in Fig. 1. In this figure, the targets and propagation paths showing below the ionosphere layer are physically present, whereas those above the ionosphere layer are their images due to ionosphere and ground reflections and are included in the figure for convenience of slant-range calculation.

The OTHR signals reflected by the target and received at the radar receivers follow multiple round-trip paths due to their reflections from the ionosphere and the earth surface [8, 13]. As illustrated in Fig. 1, the specular earth and ionosphere reflections result in two different propagation paths for each of the transmit and receive OTHR signals, yielding three distinct round-trip paths. For the first round-trip path, both transmit and receive OTHR signals propagate along Path I, denoted as $[l_1, l_1]$. Similarly, the second round-trip path $[l_2, l_2]$ follows Path II for both ways. The third round-trip path uses different forward and return paths, i.e., $[l_1, l_2]$ and $[l_2, l_1]$.

In Fig. 1, H is the height of the ionosphere layer which

The work of Y. D. Zhang is supported in part by a contract with Altamira Technologies Corp. for research sponsored by the Air Force Research Laboratory under Contract FA8650-18-C-1055.

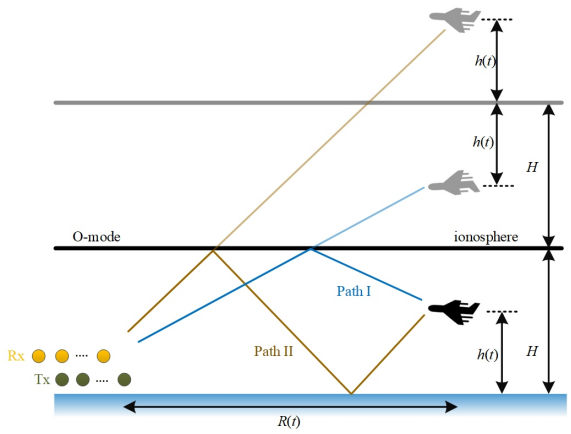

Fig. 1: Flat-earth local multipath propagation model of OTHR.

is assumed constant and its coarse estimate is available from ionosonde monitoring, and h is an unknown target altitude to be estimated. In addition, the target range R_t is time-varying with velocity v_t, i.e.,

$$R_t = R_0 + \int_0^t v_t \mathrm{d}t. \tag{1}$$

We first consider the case with a constant velocity, i.e., $v_t = v_0$ and thus

$$R_t = R_0 + v_0 t. \tag{2}$$

We will then consider several cases with different time-varying velocity patterns.

From Fig. 1, we can calculate the one-way slant ranges $l_t^{(1)}$ and $l_t^{(2)}$ of Path I and Path II in terms of the ionosphere height H, target range R_t, and target altitude h, as [8]:

$$l_t^{(1)} = \left(R_t^2 + (2H-h)^2\right)^{\frac{1}{2}} = R_t\left(1 + \frac{4H^2 + h^2 - 4Hh}{R_t^2}\right)^{\frac{1}{2}}, \tag{3a}$$

$$l_t^{(2)} = \left(R_t^2 + (2H+h)^2\right)^{\frac{1}{2}} = R_t\left(1 + \frac{4H^2 + h^2 + 4Hh}{R_t^2}\right)^{\frac{1}{2}}, \tag{3b}$$

In order to gain insightful observations of the relationship between the Doppler frequencies and the target motion, we exploit the first-order Taylor series expansion of Eq. (3) for approximation. Under the commonly satisfied assumption $R_t \gg H \gg h$, we obtain the following simplified expressions of the one-way slant ranges:

$$l_t^{(1)} \approx R_t + \frac{2H}{R_t}(H-h), \quad l_t^{(2)} \approx R_t + \frac{2H}{R_t}(H+h). \tag{4}$$

B. Multipath Doppler Signatures

The slant ranges of the three round-trip paths (Path I: $[l_t^{(1)}, l_t^{(1)}]$, Path II: $[l_t^{(2)}, l_t^{(2)}]$, and Path III: $[l_t^{(1)}, l_t^{(2)}]$ or $[l_t^{(2)}, l_t^{(1)}]$) are respectively represented as:

$$L_t^{(1)} = 2l_t^{(1)}, \quad L_t^{(2)} = 2l_t^{(2)}, \quad L_t^{(3)} = l_t^{(1)} + l_t^{(2)}. \tag{5}$$

The Doppler signatures corresponding to the three round-trip paths can be expressed as:

$$\nu_t^{(i)} = -\frac{f_c}{c}\frac{\mathrm{d}L_t^{(i)}}{\mathrm{d}t} = -\frac{\mathrm{d}L_t^{(i)}}{\lambda \mathrm{d}t}, \qquad i = 1, 2, 3, \tag{6}$$

where f_c is the carrier frequency of the OTHR signal, c is the velocity of the electromagnetic wave, and $\lambda = c/f_c$ denotes the signal wavelength.

III. Target Doppler Characteristics

In this section, we investigate the micro-multipath Doppler frequencies of a target and the effect of variation in the target velocity. We first assume that the target is moving at a constant velocity $\dot{R}_t = \dot{R} = v_0$, and the effect of the variation of target velocity on the resulting Doppler signatures is then examined by exploiting a time-varying velocity $\dot{R}_t$.

A. Target with a Constant Velocity

In this section, we will keep using $\dot{R}$ instead of v_0 to make the results more conveniently modified to a time-varying velocity case in the following subsections. Note that the target velocity $\dot{R}$ takes a positive value when the target range increases with time, i.e., it moves away from the radar.

Using the approximations in Eq. (4), the derivatives of the one-way slant ranges are expressed as:

$$\frac{\mathrm{d}l_t^{(1)}}{\mathrm{d}t} \approx \dot{R} - \frac{2H\dot{R}}{R_t^2}(H-h), \quad \frac{\mathrm{d}l_t^{(2)}}{\mathrm{d}t} \approx \dot{R} - \frac{2H\dot{R}}{R_t^2}(H+h). \tag{7}$$

Using Eq. (6), we can find the Doppler frequencies due to the three round-trip paths as:

$$\nu_t^{(1)} = \bar{\nu}_t + \Delta\nu_t, \quad \nu_t^{(2)} = \bar{\nu}_t - \Delta\nu_t, \quad \nu_t^{(3)} = \bar{\nu}_t, \tag{8}$$

where

$$\bar{\nu}_t = -\frac{\mathrm{d}(l_t^{(1)} + l_t^{(2)})}{\lambda \mathrm{d}t} \approx -\frac{2}{\lambda}\dot{R} + \frac{4H^2}{\lambda R_t^2}\dot{R} \tag{9}$$

is termed as the nominal Doppler frequency, and

$$\Delta\nu_t = -\frac{\mathrm{d}(l_1 - l_2)}{\lambda \mathrm{d}t} \approx \frac{4Hh}{\lambda R_t^2}\dot{R} \tag{10}$$

is referred to as the Doppler frequency difference between the micro-Doppler components. It is noted from Eqs. (9) and (10) that the target altitude information is more closely related to the Doppler frequency difference $\Delta\nu_t$.

Under the previous assumption $R_t \gg H \gg h$, the first term at the right-hand side of (9) contributes a dominant Doppler frequency with a constant value, whereas the second term at the right-hand side of (10) contributes a much smaller value to the Doppler frequency, which is assumed to vary slowly with time as it depends on R_t^2.

To clearly observe the time-dependency of the Doppler signatures, we use a Taylor series expansion to approximate $1/R_t^2$ as

$$\frac{1}{R_t^2} \approx \frac{1}{R_0^2} - \frac{2}{R_0^3}\dot{R}t. \tag{11}$$

Therefore, $\bar{\nu}_t$ becomes

$$\bar{\nu}_t \approx -\frac{2}{\lambda}\dot{R} + \frac{4H^2}{\lambda R_0^2}\dot{R} - \frac{8H^2}{\lambda R_0^3}\dot{R}^2 t. \tag{12}$$

It is clear that this is a chirp Doppler signature and, interestingly, the chirp rate, given as $-8H^2\dot{R}^2/(\lambda R_0^3)$, is always negative for the scenario with a constant-velocity target, regardless of the direction of the target motion.

When considering the term $\Delta\nu_t$ given in (10), and because the variation of R_t is very small, i.e., $|\dot{R}t| \ll R_0$, it can be approximated as a constant, i.e., $R_t \approx R_0$. Thus, we have

$$\Delta\nu_t \approx \frac{4Hh}{\lambda R_t^2}\dot{R} \approx \frac{4Hh}{\lambda R_0^2}\dot{R} := \Delta\nu. \tag{13}$$

As a result, it becomes clear that the Doppler signatures for the round-trip paths I and II are symmetric and wrap around the Doppler signature of the round-trip path III. The average Doppler component, $\bar{\nu}_t$, is a chirp that is shared by all three round-trip paths, whereas the small frequency difference between the Doppler signatures corresponding to different paths can be treated as a constant, denoted as $\Delta\nu$.

B. Target with Time-Varying Constant Acceleration

When the constant velocity of a target is perturbed, the instantaneous Doppler signature will deviate from the parallel LFM model. Consider a general model in which the instantaneous target velocity is described as

$$\dot{R}_t = v_0 + \int_0^t a_t \mathrm{d}t := v_0 + \Delta\dot{R}_t, \tag{14}$$

where a_t is the instantaneous acceleration. In this case, the nominal Doppler frequency is obtained as

$$\begin{aligned}\bar{\nu}_t &\approx -\frac{2}{\lambda}\dot{R}_t + \frac{4H^2}{\lambda R_0^2}\dot{R}_t - \frac{8H^2}{\lambda R_0^3}\dot{R}_t^2 t \\ &= -\frac{2}{\lambda}(v_0+\Delta\dot{R}_t) + \frac{4H^2}{\lambda R_0^2}(v_0+\Delta\dot{R}_t) - \frac{8H^2}{\lambda R_0^3}(v_0+\Delta\dot{R}_t)^2 t.\end{aligned} \tag{15}$$

Typical aircraft velocity fluctuations are much smaller than the aircraft velocity [27], that is, $|\Delta\dot{R}_t| \ll |v_0|$. Therefore, when $|a(t)| \geq 4H^2 v_0^2/R_0^3$, the instantaneous slope of the nominal Doppler frequency $\bar{\nu}_t$, that is, $\mathrm{d}\bar{\nu}_t/\mathrm{d}t$, is dominated by $-2a(t)/\lambda$. As a result, the Doppler signatures depend on the perturbation patterns and will likely deviate from the LFM model described in (13). Two examples will be described in Sections IV and V.

On the other hand, the Doppler difference between the three multipath Doppler components becomes

$$\Delta\nu_t \approx \frac{4Hh}{\lambda R_0^2}\dot{R}_t = \frac{4Hh}{\lambda R_0^2}(v_0 + \Delta\dot{R}_t) \approx \frac{4Hh}{\lambda R_0^2}v_0 := \Delta\nu. \tag{16}$$

The last approximation is rendered from $|\Delta\dot{R}_t| \ll |v_0|$ as discussed above.

In summary, for target perturbation due to turbulence, the main impact to the Doppler signature is the change of the Doppler slope which is shared by the three micro-multipath components, whereas its impact on the Doppler difference is insignificant so that micro-Doppler signatures can still be considered parallel in the time-frequency domain.

Such observations reveal that, when the target altitude is concerned, instead of directly estimating the three Doppler signatures, it is much simpler to estimate the Doppler difference. The self-stationarization technique reported in [28] is useful for the estimation of the Doppler difference without the need to consider the variation in the nominal Doppler frequency. Because all Doppler signatures of the micro-multipath signals are parallel, the self-stationarization results in the sinusoidal output for convenience of analysis of the difference Doppler frequency. The target altitude can be obtained from (16) using coarse estimate of the target range and velocity, which are much easier to obtain.

TABLE I: Key Parameters (unless otherwise specified)

Parameter	Notation	Value
Initial range	R_0	2,500 km
Ionosphere height	H	350 km
Target altitude	h	20 km
Target initial velocity	v_0	-300 m/sec
Carrier frequency	f_c	16 MHz
Pulse repetition frequency	f_s	140 Hz
Signal-to-noise ratio	SNR	-10 dB
Coherent processing interval	T	30 s

IV. Doppler Signature Stationarization and Analysis

Under this assumption, the received signal can be expressed as [28, 29]:

$$x_t = A^{(1)}\exp(j\phi_t^{(1)}) + A^{(2)}\exp(j\phi_t^{(2)}) + A^{(3)}\exp(j\phi_t^{(3)}), \tag{17}$$

where $A^{(i)}$ and $\phi_t^{(i)}$ are, respectively, the path loss and the instantaneous phase of the ith path for $i = 1, 2$, and 3.

The instantaneous phases can be expressed as

$$\phi_t^{(i)} = -2\pi\int_0^t \nu_t^{(i)}\mathrm{d}t = -2\pi\int_0^t \left(\bar{\nu}_t + \xi^{(i)}\Delta\nu\right)\mathrm{d}t, \tag{18}$$

where $\xi^{(1)} = 1$, $\xi^{(2)} = -1$, and $\xi^{(3)} = 0$.

For clarity, we denote $\theta_t = -2\pi\int_0^t \bar{\nu}_t\mathrm{d}t$ and $\psi_t = -2\pi\int_0^t \Delta\nu\mathrm{d}t$. Then, (18) can be written as

$$\phi_t^{(1)} = \theta_t + \psi_t, \quad \phi_t^{(2)} = \theta_t - \psi_t, \quad \phi_t^{(3)} = \theta_t. \tag{19}$$

Signal self-stationarization is achieved by multiplying x_t with its conjugation, x_t^*, resulting in

$$\begin{aligned}|x_t|^2 &= x_t x_t^* \\ &= \left(|A_1|^2 + |A_2|^2 + |A_3|^2\right) \\ &+ (A_1A_3^* + A_2^*A_3)\exp(-j\psi_t) \\ &+ (A_1^*A_3 + A_2A_3^*)\exp(j\psi_t) \\ &+ A_1A_2^*\exp(-j2\psi_t) + A_1^*A_2\exp(j2\psi_t).\end{aligned} \tag{20}$$

It is clear from the above expression that the resulting product $|x_t|^2$ does not depend on θ_t. It contains DC component, $\pm\psi_t$, and $\pm2\psi_t$. As a result, the effect of Doppler variation due to the target velocity perturbation vanishes, thereby enabling robust estimation of the Doppler difference. In particular, in the underlying problem, as ψ_t is obtained from constant Doppler difference $\Delta\nu$, $|x_t|^2$ renders five constant frequency components, namely, 0, $\pm\Delta\nu$, and $\pm2\Delta\nu$. Such results can be easily solved using Fourier transform or sparsity-based line spectrum estimation methods.

To provide improved visualization and estimation of the Doppler difference of interest, two post-processing steps are carried out. First, we remove the dominant DC component through the subtraction of the signal average component. Second, we fuse the information contained in the four harmonic non-zero frequency signatures to enhance the desired

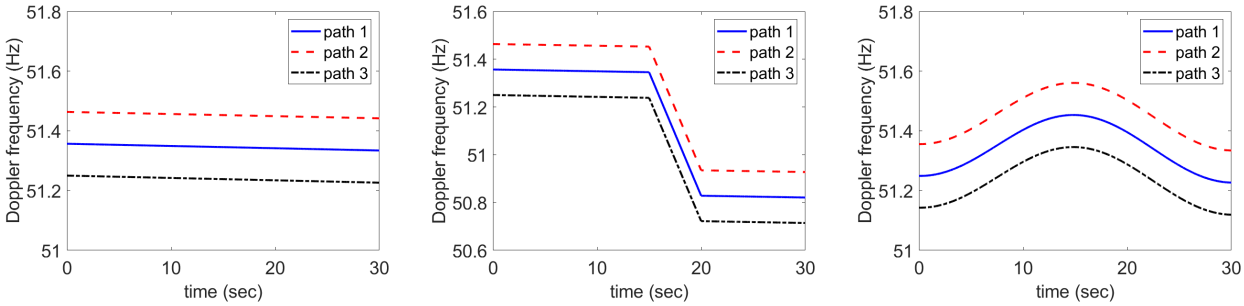

(a) Constant velocity (b) Change velocity in 5 s (c) Velocity varies sinusoidally

Fig. 2: Doppler signatures of the three micro-multipath components.

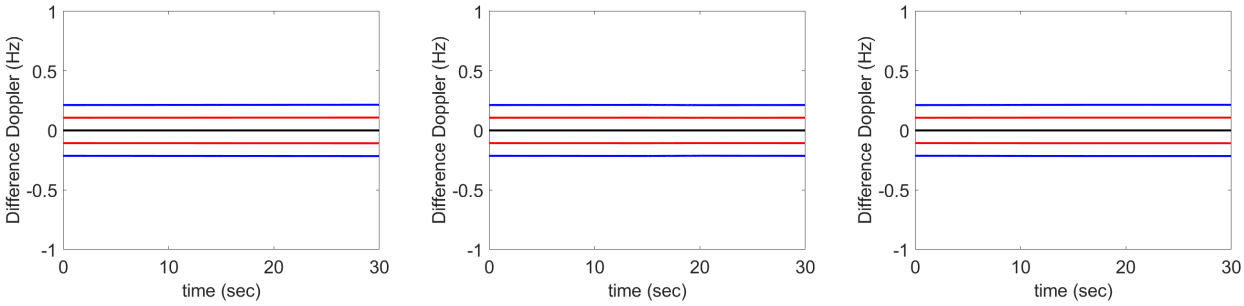

(a) Constant velocity (b) Change velocity in 5 s (c) Velocity varies sinusoidally

Fig. 3: Different Doppler frequencies obtained after performing self-stationarization.

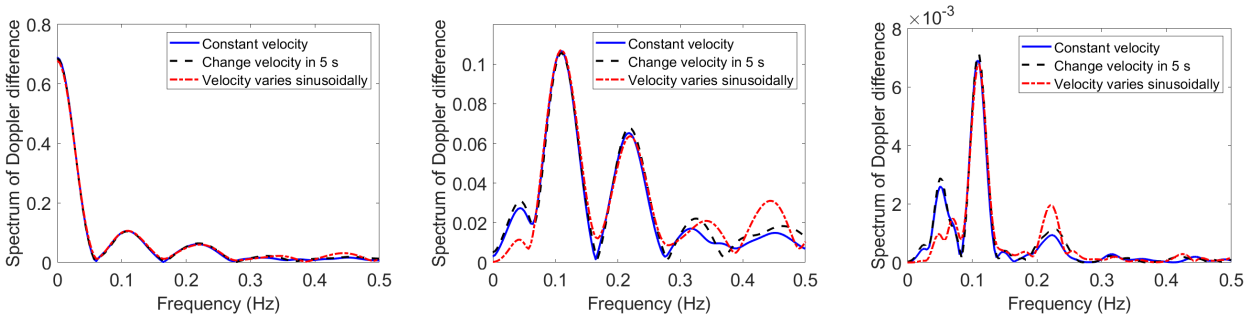

(a) Without DC removal (b) With DC removal (c) After signature enhanced

Fig. 4: Fourier-based Doppler frequency difference estimation.

component of $\Delta\nu$. Denote $X(f)$ as the spectrum of $|x_t|^2$, we compute the following quantity:

$$Y(f) = |X(f)X(f/2)|. \tag{21}$$

Because the spectrum are symmetric, only the positive frequency needs to be considered and processed.

V. Simulation Results

Consider a target flying at a constant altitude, and the other key parameters are listed in Table I. Note that the input signal-to-noise ratio (SNR) included the array gain offered by the OTHR which is typically operated in a multiple-input multiple-output (MIMO) radar mode.

To show the effectiveness of the proposed method, we first show the Doppler signatures for three different scenarios: (1) Target with a constant velocity is considered as a baseline; (2) Target velocity varies from -500 m/s to -495 m/s during a 5-second time period between $15 \leq t \leq 20$ s; (3) Target velocity varies in a sinusoidal manner with maximum velocity deviation of 5 m/s. The resulting Doppler signatures are illustrated in Fig. 2. The depicted signatures confirm our earlier analyses that the Doppler signatures are no longer LFM but the Doppler differences between them remain approximately constant. Fig. 3 shows the Doppler difference obtained from the stationarized signal $|x_t|^2$. It is clear that the three cases render the same Doppler difference with indistinguishable variations.

Fig. 4(a) shows the simulated spectrum of the Doppler difference for the three cases. A Hamming window is applied to the entire data length to reduce the sidelobe levels. All three cases render similar results. Fig. 4(b) shows the result after the removal of the dominant DC component to better represent

the desired Doppler difference components and avoid potential bias due to the DC component. Fig. 4(c) shows the enhanced spectrum using Eq. (21) where the desired Doppler difference is enhanced. From Figs. 4(b) and 4(c), the Doppler difference corresponding to the peak spectrum values is obtained as 0.11 Hz for all the three cases. Based on this Doppler difference estimate, the target altitude h is estimated as 18.42 km which is very close to the actual target altitude of 20 km. The difference is mainly due to the Taylor series approximation.

VI. Conclusion

In this paper, we have analyzed the Doppler frequency characteristics of target signals in OTHR when the target velocity varies due to, for example, turbulence. Noticing that the velocity variation changes the Doppler signatures of all micro-multipath components in a similar manner, we apply the self-stationarization approach which enables robust estimation of the Doppler difference between these micro-multipath components, and the results are used to further estimate the target altitude. The proposed technique handles different patterns of target velocity variation.

VII. References

[1] M. Headrick and M. I. Skolnik, "Over-the-horizon radar in the HF band," *Proc. IEEE*, vol. 62, no. 6, pp. 664–673, June 1974.

[2] Y. Zhang, G. J. Frazer, and M. G. Amin, "Concurrent operation of two over-the-horizon radars," *IEEE J. Sel. Topics Signal Process.*, vol. 1, no. 1, pp. 114–123, June 2007.

[3] G. J. Frazer, Y. Abramovich, B. A. Johnson, "Use of adaptive non-causal transmit beamforming in OTHR: Experimental results," in *Proc. Int. Conf. Radar*, Adelaide, Australia, Sept. 2008, pp. 311–316.

[4] J. M. Headrick and S. J. Anderson, "HF over-the-horizon radar," Chapter 20 in M. Skolnik (ed.), *Radar Handbook, 3rd Ed.* McGraw-Hill, 2008.

[5] G. A. Fabrizio, *High Frequency Over-the-Horizon Radar: Fundamental Principles, Signal Processing, and Practical Applications*. McGraw-Hill, 2013.

[6] M. Papazoglou and J. L. Krolik, "Matched-field estimation of aircraft altitude from multiple over-the-horizon radar revisits," *IEEE Trans. Signal Process.*, vol. 47, no. 4, pp. 966–976, April 1999.

[7] R. H. Anderson, S. Kraut, and J. L. Krolik, "Robust altitude estimation for over-the-horizon radar using a state-space multipath fading model," *IEEE Trans. Aerospace Electron. Syst.*, vol. 39, no. 1, pp. 192–201, Mar. 2003.

[8] Y. D. Zhang, M. G. Amin, and G. J. Frazer, "High-resolution time-frequency distributions for manoeuvring target detection in over-the-horizon radars," *IEE Proc.-Radar Sonar Navig.*, vol. 150, no. 4, pp. 299–304, Aug. 2003.

[9] K. Lu, and X. Liu, "Enhanced visibility of maneuvering targets for high-frequency over-the-horizon radar," *IEEE Trans. Antennas Propag.*, vol. 53, no. 1, pp. 404–411, Jan. 2005.

[10] K. Bell, "MAP-PF multi-mode tracking for over-the-horizon radar," in *Proc. IEEE Radar Conf.*, Atlanta, GA, May 2012, pp. 326–331.

[11] M. Papazoglou and J. L. Krolik, "Estimation of aircraft altitude and altitude rate with over-the-horizon radar," in *Proc. IEEE Int. Conf. Acoust. Speech Signal Process.,*, Phoenix, AZ, March 1999, pp. 2103–2106.

[12] J. Praschifka, L. J. Durbridge and J. Lane, "Investigation of target altitude estimation in skywave OTH radar using a high-resolution ionospheric sounder," in *Proc. Intl. Radar Conf.*, Bordeaux, France, Oct. 2009, pp. 1–6.

[13] Y. D. Zhang, J. J. Zhang, M. G. Amin, and B. Himed, "Instantaneous altitude estimation of maneuvering targets in over-the-horizon radar exploiting multipath Doppler signatures," *EURASIP J. Adv. Signal Process.*, vol. 2013, no. 2013:100, pp. 1–13, May 2013.

[14] V. S. Amin, Y. D. Zhang, and B. Himed, "Group sparsity-based local multipath Doppler difference estimation in over-the-horizon radar," in *Proc. IEEE Int. Radar Conf.*, Rockville, MD, April-May 2020.

[15] C. Ioana, Y. D. Zhang, M. G. Amin, F. Ahmad, and B. Himed, "Time-frequency analysis of multipath Doppler signatures of maneuvering targets," in *Proc. IEEE Int. Conf. Acoust. Speech Signal Process.*, Kyoto, Japan, March 2012.

[16] C. Ioana, Y. D. Zhang, M. G. Amin, F. Ahmad, G. Frazer, and B. Himed, "Time-frequency characterization of micro-multipath signals in over-the-horizon radar," in *Proc. IEEE Radar Conf.*, Atlanta, GA, May 2012, pp. 671–675.

[17] Y. D. Zhang, M. G. Amin, and B. Himed, "Direction-of-arrival estimation of nonstationary signals exploiting signal characteristics," in *Proc. Int. Conf. Inform. Science, Signal Process., and Their Appli.*, Montreal, Canada, July 2012.

[18] C. Hou, Y. Wang, and J. Chen, "Estimating target heights based on the earth curvature model and micro-multipath effect in skywave OTH radar," *J. Applied Math.*, vol. 2014, article ID 424191, pp. 1–14, 2014.

[19] A. Ahmed, Y. D. Zhang, and B. Himed, "Doppler signature analysis of mixed O/X-mode signals in over-the-horizon radar," in *Proc. IEEE Int. Radar Conf.*, Rockville, MD, April 2020.

[20] A. Ahmed, Y. D. Zhang, and B. Himed, "Doppler signature separation of mixed O/X-mode over-the-horizon radar signals," in *Proc. IEEE Radar Conf.*, Florence, Italy, Sep. 2020.

[21] Y. D. Zhang, A. Ahmed, and B. Himed, "Target altitude estimation in over-the-horizon radar," *IEEE Access*, vol. 10, pp. 11260–11273, Jan. 2022.

[22] A. Ahmed, Y. D. Zhang, and B. Himed, "Joint target and ionosphere parameter estimation in over-the-horizon radar," *IEEE Trans. Aerospace Electron. Syst.*, in press. doi: 10.1109/TAES.2022.3161396.

[23] H. M. Ozaktas, M. A. Kutay, and Z. Zalevsky, *The Fractional Fourier Transform: With Applications in Optics and Signal Processing*. Wiley, 2001.

[24] E. Sejdić, I. Djurović, and L. Stanković, "Fractional Fourier transform as a signal processing tool: An overview of recent developments," *Signal Process.*, vol. 91, no. 6, pp. 1351–1369, June 2011.

[25] B. Raghavan and N. Ananthkrishnan, "Small-perturbation analysis of airplane dynamics with dynamic stability derivatives redefined," in *AIAA Atmosph. Flight Mech. Conf. Exhibit*, San Francisco, CA, Aug. 2005.

[26] Y. Wang and B. Geerts, "Estimating the evaporative cooling bias of an airborne reverse flow thermometer," *J. Atmos. Oceanic Technol.*, vol. 26, no. 1, pp. 3–21, Jan. 2009.

[27] Brazil National Civil Aviation Agency, "Turbulence." Available at https://www.anac.gov.br/en/safety/aeronautical-meteorology/conditions/turbulence

[28] Y. D. Zhang and B. Himed, "Multipath Doppler difference estimation in over-the-horizon radar," in *Proc. IEEE Radar Conf.*, Oklahoma City, OK, April 2018.

[29] V. S. Amin, Y. D. Zhang, and B. Himed, "Modified Viterbi-based local-multipath Doppler difference estimation in over-the-horizon radar," in *Proc. Asilomar Conf. Signals, Systems, and Computers*, Pacific Grove, CA, Nov. 2021.